Environmental Research 251 (2024) 118595

Contents lists available at ScienceDirect

Environmental Research

journal homepage: www.elsevier.com/locate/envres

Synthesis of sustainable mesoporous sulfur-doped biobased carbon with superior performance sodium diclofenac removal: Kinetic, equilibrium, thermodynamic and mechanism

Glaydson S. dos Reis [a,*], Alejandro Grimm [a], Denise Alves Fungaro [b], Tao Hu [c], Irineu A.S. de Brum [d], Eder C. Lima [e], Mu Naushad [f], Guilherme L. Dotto [g], Ulla Lassi [c]

[a] Department of Forest Biomaterials and Technology, Biomass Technology Centre, Swedish University of Agricultural Sciences, Umeå, SE-901 83, Sweden
[b] Instituto de Pesquisas Energéticas e Nucleares (IPEN / CNEN -SP)Av. Professor Lineu Prestes 224205508-000, São Paulo, SP, Brazil
[c] Research Unit of Sustainable Chemistry, University of Oulu, P.O. Box 3000, FI-90014, Oulu, Finland
[d] Mineral Processing Laboratory, Federal University of Rio Grande do Sul, 9500 Bento Gonçalves Avenue, Porto Alegre, 91501-970, Brazil
[e] Institute of Chemistry, Federal University of Rio Grand do Sul (UFRGS), Porto Alegre, RS, Brazil
[f] Department of Chemistry, College of Science, King Saud University, P.O. Box 2455, Riyadh, Saudi Arabia
[g] Research Group on Adsorptive and Catalytic Process Engineering (ENGEPAC), Federal University of Santa Maria, Av. Roraima, 1000-7, 97105–900, Santa Maria, RS, Brazil

ARTICLE INFO

Keywords:
Heteroatom doping
Sulfur-doped biochar
Fast adsorption's kinetic

ABSTRACT

Over the last years, the strategy of employing inevitable organic waste and residue streams to produce valuable and greener materials for a wide range of applications has been proven an efficient and suitable approach. In this research, sulfur-doped porous biochar was produced through a single-step pyrolysis of birch waste tree in the presence of zinc chloride as chemical activator. The sulfur doping process led to a remarkable impact on the biochar structure. Moreover, it was shown that sulfur doping also had an important impact on sodium diclofenac (S-DCF) removal from aqueous solutions due to the introduction of S-functionalities on biochar surface. The adsorption experiments suggested that General and Liu models offered the best fit for the kinetic and equilibrium studies, respectively. The results showed that the kinetic was faster for the S-doped biochar while the maximum adsorption capacity values at 318 K were 564 mg g^{-1} (non-doped) and 693 mg g^{-1} (S-doped); highlighting the better affinity of S-doped biochar for the S-DCF molecule compared to non-doped biochar. The thermodynamic parameters (ΔH^0, ΔS^0, ΔG^0) suggested that the S-DCF removal on both adsorbents was spontaneous, favourable, and endothermic.

1. Introduction

The rapid expansion of industrial activities has also been accompanied by many environmental problems due to the continuous depletion of fossil-based resources and the large generation of wastes that pose a serious threat to human existence in the foreseeable future. For instance, the World has faced issues related to the pollution of water bodies for a long time due to anthropogenic activities (Ojha et al., 2017; Jayaswal et al., 2018; Owa, 2013; Schweitzer and Noblet, 2018). Moreover, pollution of waters by traces of pharmaceuticals in water bodies has posed serious concerns among stakeholders such as government, water regulators, water suppliers, and civil society regarding possible dangers of drinking waters containing traces of pharmaceuticals (Zuccato et al., 2008; Kümmerer, 2001). Therefore, these must be properly removed from wastewaters before entering the natural water bodies.

Several treatment methods can be employed in the removal of pharmaceuticals from wastewaters including biological processes (Dionisi and Etteh, 2019), photo-fenton process (Della-Flora et al., 2020), filtration (Ahsani et al., 2020), coagulation (Zahrim et al., 2019), photocatalysis (Kovacic et al., 2020), and adsorption (dos Reis et al., 2023a; Gonzalez-Hourcade et al., 2022; dos Reis et al., 2023b; dos Reis et al., 2022a,b). However, the majority of these approaches require high costs of implementation and operation as well as high use of chemicals, which elevate the costs of the process; besides, huge amounts of by-products and sludge can be generated, requiring further treatment. Among the aforementioned treatment methods, adsorption could be considered a

* Corresponding author.
E-mail address: glaydson.simoes.dos.reis@slu.se (G. S. dos Reis).

https://doi.org/10.1016/j.envres.2024.118595
Received 27 December 2023; Received in revised form 16 February 2024; Accepted 28 February 2024
Available online 9 March 2024

very suitable one due to its simplified operation, high efficiency, low-cost process, and no generation of by-products (including sludge), and the possibility of regenerating the adsorbent after exhaustive use, including its post-uses in other applications such anodes for battery application (Yu et al., 2021).

The efficiency of the adsorption method is severely dependent on the adsorbent characteristics (dos Reis et al., 2022a,b). By far, activated carbons/biochars are the most known and employed adsorbents, thanks to their physicochemical characteristics such as high specific surface areas and a large number of functionalities on its surfaces, which are important features for high/performance adsorbents (Lima et al., 2022). Biochars can be synthesized by pyrolysis from different biomass precursors, which are sustainable resources, owing advantages of improving the circularity of the biomass wastes, promoting sustainable approaches for materials syntheses, which has an impact on reducing the CO_2 footprint (Lima et al., 2022). Another advantage of biomass-based carbon materials is that they can be easily functionalized/modified through an easy method called "heteroatom doping", which is the introduction of heteroatoms (e.g., nitrogen, oxygen, boron, sulfur, and phosphorus) into the graphitic carbon structure to improve their physicochemical and adsorptive properties (dos Reis et al., 2023a,b).

Among the heteroatoms, nitrogen is the most employed one to dope biochars (dos Reis et al., 2023b; Li et al., 2019). However, sulfur also appears as an efficient strategy to modify biochar structure (Gao et al., 2021; Alimohammadi et al., 2022). The sulfur electronegativity is 2.58, which is close to that of carbon (2.55) and therefore will not create a huge imbalance in the electronegativity of the doped carbons but would change the electron distribution, and produce structural defects of carbon layers, which are the reaction sites for boosting adsorptive properties (Gao et al., 2021; Du et al., 2020). Doping with sulfur can reduce the energy gap between molecular orbitals, form thiophene groups and enhance the reactivity of catalysts to electron acceptors (Du et al., 2020; Xie et al., 2023a, b), which could also boost its adsorptive properties. Moreover, the strategy of using S as dopant is more interesting due to the sulfur large reserves worldwide, low cost, and being environmentally friendly compared to other heteroatoms and toxic transition metals.

In this work, sulfur-doped biochar was prepared using wastes generated from the harvesting of birch trees (Betula spp.) as a sustainable precursor. The Betula spp. Includes several species of trees that are heavily widespread in the Northern Hemisphere (Hynynen et al., 2010). Pure sulfur was used as dopant with the doping/activation of the biochars done using single-step pyrolysis. To understand the S-doping process on the physicochemical characteristics of the S-doped biochar, several physicochemical characterization techniques were employed, and a non-doped biochar was prepared and used for comparison. The biochar samples were used to remove sodium diclofenac (S-DCF) from water as well as to remove contaminants from synthetic effluents made of several dyes and inorganic pollutants usually present in wastewater.

Among several pharmaceuticals, sodium diclofenac is one of the most used worldwide anti-inflammatory drugs and due to its recalcitrant features, it is poorly removed in conventional wastewater treatment, therefore the employment of new materials to remove it is highly justified. This work opens new strategies for the development of efficient adsorbents for the treatment of water/wastewater contaminated with pharmaceutical residues.

2. Materials and methods

2.1. Biochars production process

One-step pyrolysis/activation/doping was performed to prepare the biochar materials. 20.0 g of birch was mixed with 40.0 g of $ZnCl_2$ and 5.0 g of sulfur (S-doped biochar). Approximately 30 mL of distilled water was added to the mixture to obtain a homogenous paste (Lima et al., 2021). The paste was then placed in a metallic crucible and dried at 75 °C for 24 h, and then pyrolysed at 600 °C, at a heating rate of 10 °C/min, for 1 h under N_2 atmosphere (50 mL min^{-1}). After pyrolysis, the oven was turned off and left to cool down until room temperature was reached. The pyrolysed carbon samples were ground to a diameter of 200 μm, and washed with HCl 5 M solution under reflux at 80 °C for 2 h (to extract the remaining $ZnCl_2$ from the carbon matrix). Finally, the biochars were washed multiple times with boiled distilled water to remove the excessive acidity of their surfaces and dried at 75 °C for 24 h before being stored for later use.

2.2. Characterization of the biochars

The porosity data was performed from nitrogen isotherms that were obtained based on standard procedures (dos Reis et al., 2023c). The SSA values were obtained based on Brunauer–Emmett–Teller (BET) method, while the pore size distribution curves were obtained from Barrett–Joyner–Halenda (BJH) method. The elemental composition of the carbon materials was performed and obtained from a device analyser (EA-IsoLink, Thermo Fisher Scientific). Briefly, oven-dried samples (0.05 g) were used to determine the contents of C, O, H, and S. Raman spectra were obtained using a Bruker Bravo spectrometer (Bruker, Ettlingen, Germany). The spectra were obtained by scanning in the range from 800 to 2000 cm^{-1} (254 scans at 4 cm^{-1} resolution).

Hydrophobic-hydrophilic index (HI) for the non-biochar and S-doped biochar were determined according to the methodology proposed by (dos Reis et al., 2023c; dos Reis et al., 2018). To obtain the point of zero charge (pH_{pzc}) of the biochar materials, it was employed a methodology reported by (dos Reis et al., 2023a; dos Reis et al., 2023b).

X-ray diffraction (XRD) patterns were recorded using a PANalytical X'Pert Pro X-ray diffractometer (Malvern Panalytical, Almelo, The Netherlands) using standard measuring procedures. Difractograms were evaluated using the HighScore Plus software (Version 4.0) and the ICDD, PDF-4+ 2023 RDB databases.

X-ray photoelectron spectroscopy (XPS) analysis was carried out using a Thermo Fisher Scientific ESCALAB 250Xi XPS System. Measurements were done according to standard measuring procedures.

2.3. Adsorption experiments

The full experimental description of the batch adsorption tests are described in the supplementary material, as well as information about Kinetic, equilibrium, and thermodynamic calculations (see supplementary material).

3. Results and discussion

3.1. Textural properties of the biochars

One of the most important characteristics of a carbon adsorbent is its porosity features including the specific surface area and the amount of mesopores, which both usually play a huge influence on the materials' ability to adsorb organic molecules (dos Reis et al., 2023a,c; dos Reis et al., 2022a,b).

N_2 adsorption isotherm is shown in Fig. 1a, the curves show that the S-doping had an important impact on its behaviour. The S-doped biochar exhibited a more obvious hysteresis (between 0.4 and 0.9 P/P_O) which suggests more mesoporous features, while in non-doped biochar, the hysteresis is less obvious. Both isotherms also presented portions related to microporosity due to their high adsorbed amounts of N_2 at low partial pressures (dos Reis et al., 2022a,b; dos Reis et al., 2021a,b).

Therefore, both biochars exhibited combined micro-meso pores features, which is further observed by the pore size distribution curves (Fig. 1b). Again, it is obvious that the introduction of S atoms in the S-doped biochar structure generated more pores in the range of mesoporosity at the portion from 8 to 20 nm, while non-doped biochar presented small mesopores and more micropores.

These results clearly match with the N_2 isotherms. Such pore feature

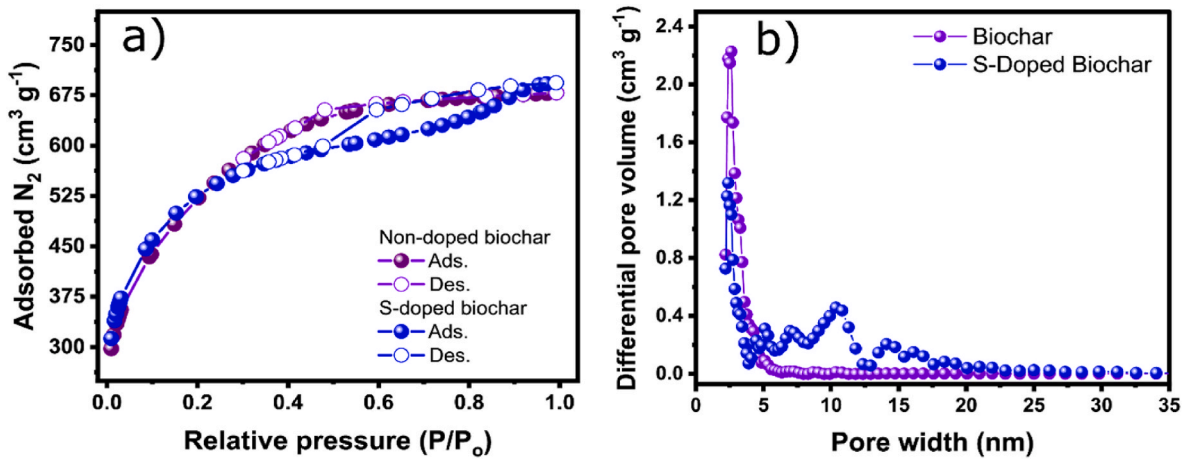

Fig. 1. a) N_2 isotherms of adsorption-desorption b) and Pore size distribution curves.

differences can have an important impact on the ability of the biochar to adsorb organic molecules because, e.g., an adsorbent rich in mesopores could positively affect the adsorption because the size of the organic molecules are in the range of mesoporosity and therefore the adsorbent pores would fit in size to "store" the organic pollutants (dos Reis et al., 2022a,b).

From the N_2 isotherms, the SSA values of the two carbons were obtained. The results show that both biochars exhibited very high SSA values regardless of the doping method, and in the SSA value, it seems that the S-doping had no effect. However, the effect of S-doping is obviously seen in the pore size effects. The percentage of mesopores in S-doped biochar is 89% while in non-doped biochar is 77% (see Table 1). These results are in agreement with the pore size distribution curves that showed more mesopore features in S-doped biochar (see Fig. 1b).

The morphology of Non-doped and S-doped biochars was examined by SEM analysis to ascertain the impact of S-doping on the materials (Fig. 2). It seems that the sulfur doping led a remarkable impact on the S-doped morphology characteristics. Non-doped biochar seems to display an intact structure with a very smoother surface with no irregular morphology such as cracks, big macropores or holes. Compared to the non-doped sample, S-doped biochar exhibits bigger sizes particles, and a rougher and irregular surface, evidencing that the incorporation of sulfur affected the morphology of the material. Such difference between both biochars may be due to the fact that the incorporation of S increased the number of defects in the biochar structure/surface which is also observed in the SEM images (Huang et al., 2021). These results are corroborated by Raman analysis which showed that S-doped biochar had more defects than non-doped. Such defective and irregular surface structure of S-doped biochar could lead to better adsorptive performances because they can act as adsorptive sites.

The contents of C, H, O, and S of the biochars are shown in Table 2. For comparison, a commercial AC possesses approximately 88% of C, 6–7% of O, around 1% of S, 0.5% of H and 0.5% of N, and 3–4% of impurities (mineral elements or ash) (Correa et al., 2017). The biochars exhibited high C contents although non-doped had higher C content, and both presented higher H content than the commercial AC. The higher presence of H could be due to the fact that biomass precursors are basically composed of hydrocarbon molecules with C–H groups.

The S-doping seems to have had a serious impact on the elemental composition of the biochars. Although the effect obvious effect on the C content, the presence of sulfur is highly evident, non-doped biochar presented only 0.152% while S-doped biochar exhibited 7.33% (wt%) of S in its structure, highlighting that the doping strategy was very efficient to introduce S atoms in the biochar matrix. The introduction of S atoms can be highly beneficial for the uptake of water contaminants due to electrostatic interactions between S-groups that act as adsorption active sites for binding molecules and ions (B. Zhang et al., 2022).

The incorporation of S in the carbon matrix caused also an impact on the surface properties of the S-doped biochar. Table 2 also shows the n-heptane/water adsorption results, from these results, the hydrophobicity/hydrophilicity index (HI) can be calculated, which indicates whether the material's surface has more hydrophobic or hydrophilic features (dos Reis et al., 2023c; dos Reis et al., 2022a,b; dos Reis et al., 2018). The results have demonstrated that the S-doping reduced the HI value of the S-doped biochar turning its surface less hydrophobic, probably due to the presence of S-functionalities that are more hydrophilic. Adsorbents with more hydrophilic surfaces are desired because it improve the contact of solid-liquid interface leading to higher adsorption performances.

The effect of S-doping was also evaluated concerning the degree of structural disorder and defects in the biochar materials. Raman spectroscopy analysis was performed in this regard. From Raman spectroscopy, I_D/I_G was calculated, recognised D (defective structure) band to G (graphitic) band intensity ratio. The smaller value for I_D/I_G means a biochar with a more orderly graphitic sheets with a higher graphitisation degree (dos Reis et al., 2022a,b; dos Reis et al., 2018; Pawlyta et al., 2015; Piergrossi et al., 2019). On the other hand, a higher I_D/I_G value means a carbon structure with a higher amount of structural defects. Therefore, Table 2 shows I_D/I_G values of 1.76 and 2.11, for the non-doped and S-doped biochar, respectively. This shows that S-doping introduced structural defects in the carbon structure which makes sense since the doping works by replacing carbon atoms with sulfur atoms and therefore boosts its defects.

Adsorbent materials with a high degree of defects can be beneficial in the adsorption process because the defects may work as adsorption sites to accommodate/bind the pollutants. Therefore, the strategy of sulfur doping may have given to the S-doped biochar, a better adsorptive performance.

The structural changes related to the sulfur doping were further evaluated by X-ray diffraction (XRD) analysis (Fig. 3). Both samples exhibit two broad diffraction peaks located at ca. 23.6° and 43.8°, corresponding to the (002) diffraction of the graphitic layer-by-layer

Table 1
Biochars surface area properties.

	SSA	A_{Micro}	A_{Meso}	% A_{Meso}	Pore volume
	(m^2 g^{-1})			(%)	(cm^3 g^{-1})
Non-doped biochar	1837 ± 26	427 ± 7	1410 ± 20	77	1.05 ± 0.017
S-doped Biochar	1809 ± 31	200 ± 3	1609 ± 26	89	1.07 ± 0.015

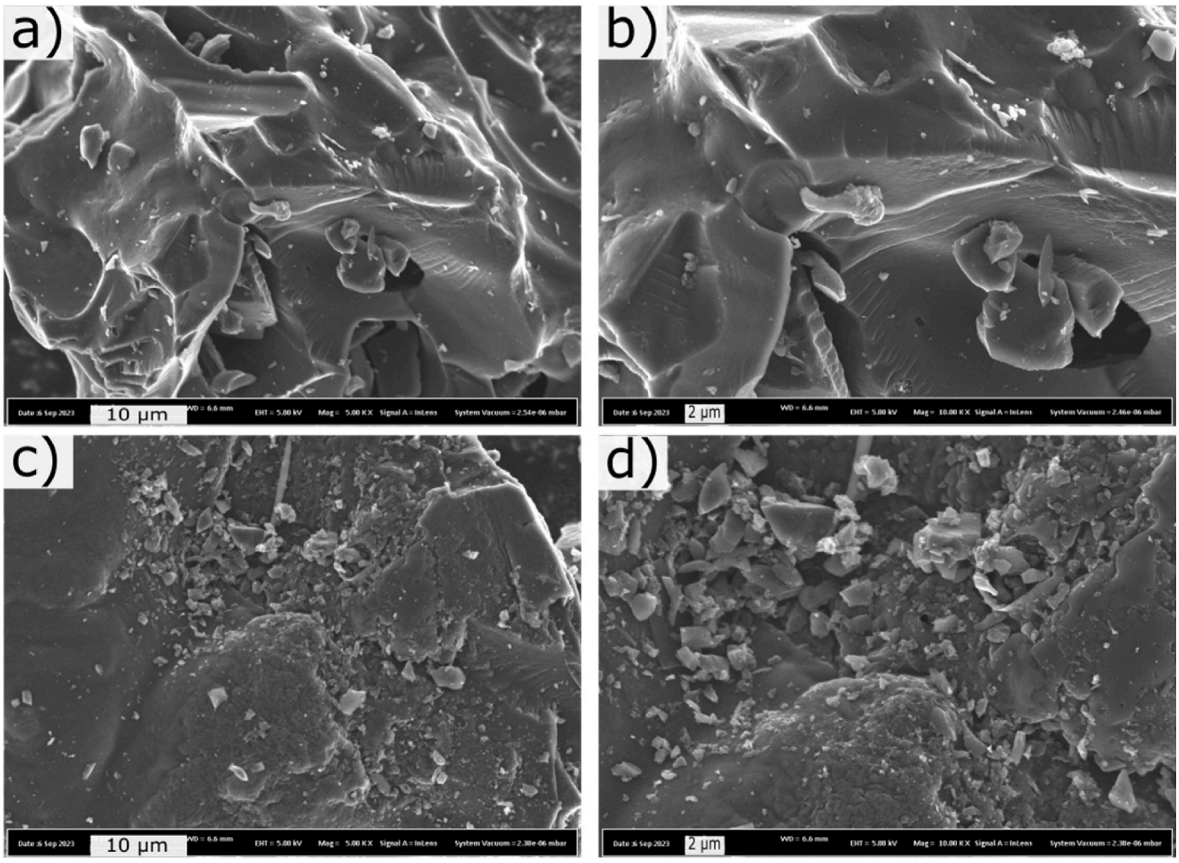

Fig. 2. SEM images of, a) non-doped biochar at 5 K, b) 10 K of magnifications, c) S-doped biochar at 5 K, and d) 10 K of magnifications.

Table 2
Physicochemical characteristics of the biochars.

	C	H	O	S	HI	I_D/I_G
Non-doped biochar	91.3	1.5	3.05	0.152	1.43	1.76
S-doped Biochar	84.7	1.2	3.25	7.33	1.02	2.11

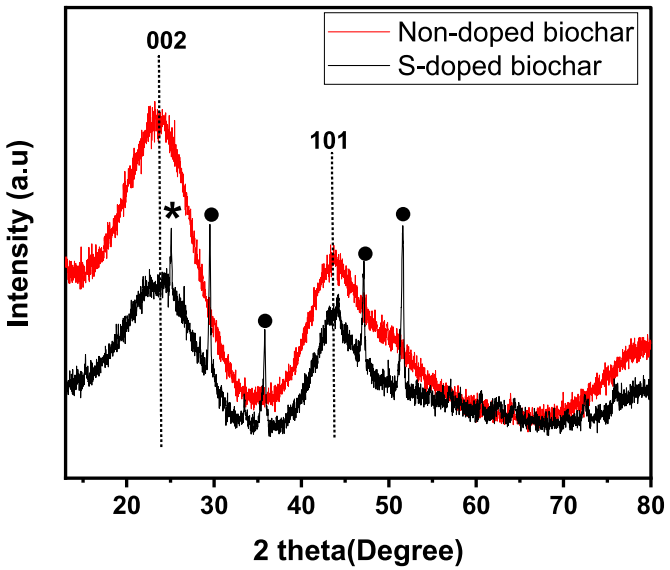

Fig. 3. XRD patterns of the biochar materials.

structure and (101) planes of graphite, respectively (Xie et al., 2023). These two peaks are more broader in Non-doped biochar, revealing its complete amorphous nature. S-doped biochar shows some crystalline sharp peaks at 2 theta of 25.1° (marked with asterisk), which matches with C_2S, Carbon Sulfide (ICDD 04-013-4391), and (marked with dosts) 29.5°, 35.8°, 47.2° and 51.6° which match with the mixture of pure sulfurs. From the analyzed results by the HighScore program, we can see the sulfurs contain α-S (ICDD 00-08-0247), β-S (ICDD 04-007-2070), Monoclinic S (ICDD 04-011-0387), and Orthorhombic S (ICDD 04-007-2096). The indication of S in physical mixture state of both amorphous and crystalline phases is because when the amount of sulfur is high, some of its particles are retained on the biochar's surface even after pyrolysis (Lai et al., 2009). The XRD patterns also confirm that the sulfur doping successfully modified the structure of S-doped biochar.

XPS analysis was employed to investigate the impact of sulfur doping on the surface chemistry, elemental compositions and sulfur-bonding configurations of the Non-doped and S-doped biochars. The XPS survey spectra (Fig. 4a) revealed the obvious presence of C and O in Non-doped biochar while in S-doped biochar the presence of C, O and S are observed, suggesting the success of the doping in incorporating sulfur atoms in the biochar carbon network. Since the sulfur was detected only in S-doped biochar its S 2p spectra was deconvoluted and four peaks are observed (Fig. 4b). The sulfur states are related to thiophene (C– S–C, 164.1 eV), sulfoxide (C–SO–C, 165.3 eV), sulfone (167.8 eV), and sulfate states (169.1 eV). The peak intensity of C–S–C bonds (thiophene) suggests that covalent carbon-sulfur-carbon bonds are the dominant state of S-doped sample.

From XPS analysis, the atomic percentage of the elements C, O and S were calculated using their respective peak areas after the deconvolution. The atomic percentage in non-doped biochar were 87.9%, and 11.9% for carbon and oxygen, respectively; while in S-doped biochar were 79.9%, 14.23% and 5.6% for carbon, oxygen and sulfur,

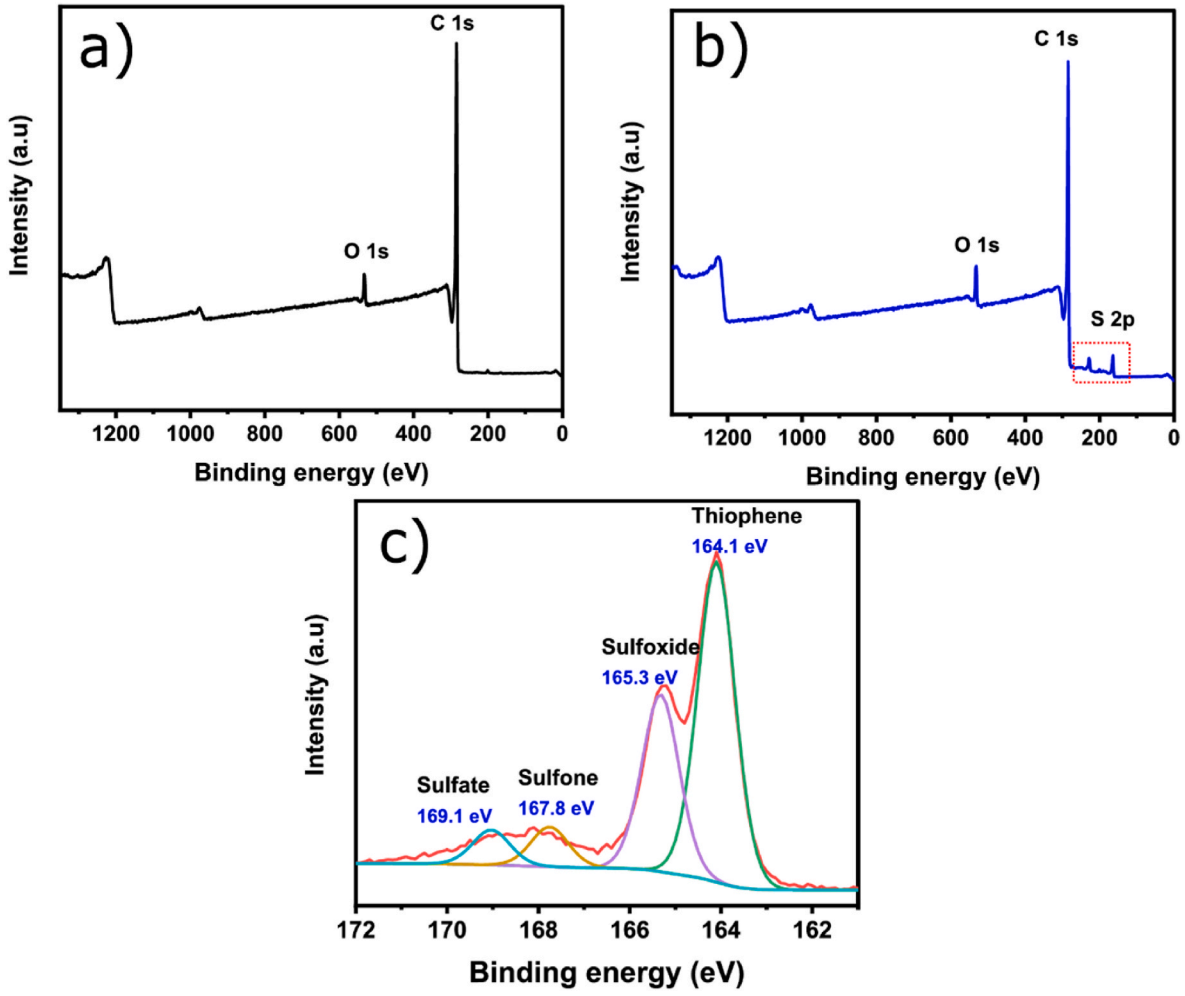

Fig. 4. a) XPS survey spectrum of non-doped biochar, b) XPS survey spectrum of S-doped biochar and c) deconvoluted S 2p peaks from S-doped biochar.

respectively. It seems that the incorporation of sulfur also led to a fixation of oxygen in the biochar structure, which means more abundance of functional groups that can boost the adsorptive properties of the material.

3.2. Point of zero charge and pH effect

The pH_{pzc} is an inherent electro-kinetic property of an adsorbent that plays a crucial influence on its adsorptive properties under certain pH conditions (dos Reis et al., 2023; dos Reis et al., 2023a,b). The point of zero charge (pH_{pzc}) of the biochars is the point where the surface charges

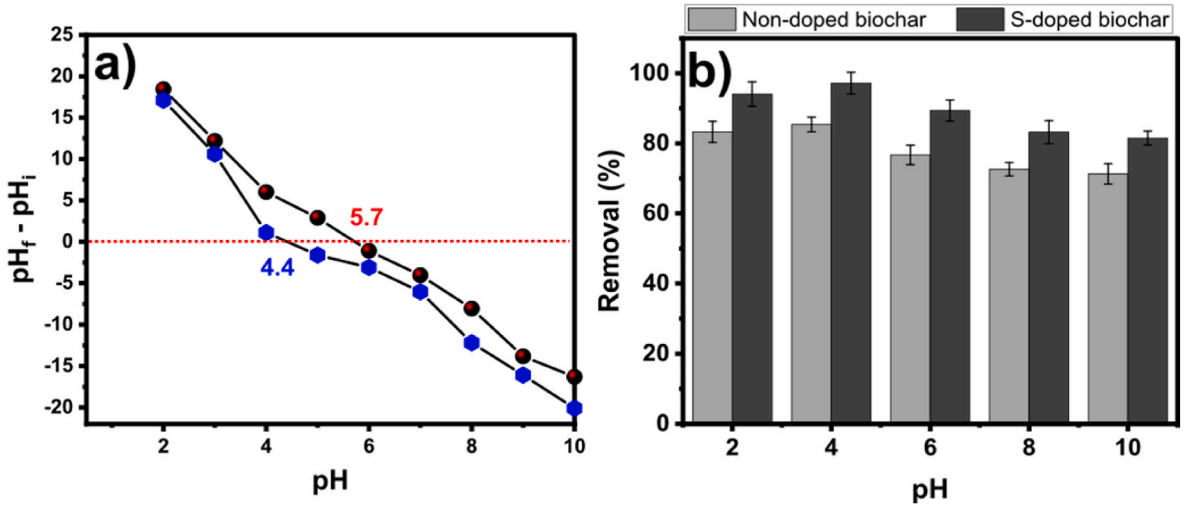

Fig. 5. a) pHpzc of the non-doped biochar and S-doped biochar samples.

are null. It provides crucial information such as that the adsorbent has its surface positively charged if the value of pH_{pzc} is below zero and negatively charged if pH_{pzc} value is above zero (dos Reis et al., 2023a; dos Reis et al., 2023b). The values of the pH_{pzc} are 4.4 (S-doped) and 5.7 (non-doped) (see Fig. 5a), indicating the acid character of the samples' surfaces but S-doped being having a more acid surface, which shows that the S-doping introduced some positive functionalities (sulfur functional groups) on S-doped biochar's surface; however, at pH higher than 4.4 (S-doped) and 5.7 (Non-doped) the surface of these carbons become negatively charged while at lower pHs these biochars' surface become positively charged. Obtained results are in agreement with results previously reported by Huang et al. (2021) that prepared S-doped carbons and the pH_{pzc} presented acid character of the samples' surfaces. The pH_{pzc} results are in total agreement with the HI data that showed that S-doped biochar exhibited lesser hydrophobic features (lower HI value) compared to non-doped carbon, possibly due to the insertion of S-functionalities that reduces hydrophobicity and increases the hydrophilicity (Kinemuchi and Ochiai, 2018).

The pH of the adsorbate-adsorbent solution plays a huge influence on the adsorption process since it affects both the speciation of the adsorbate (S-DCF) solution and the surface charge of the adsorbent (biochars). In Fig. 5b, it is possible to see how the pH influenced the S-DCF adsorption capacity of the biochars. As can be seen, for both biochars, the efficiency towards S-DCF removal did not vary much in the pH range from 2 to 10 (see Fig. 5b). The association constant value (pKa) of S-DCF is around 4.35, which means that S-DCF stays as unionized form below 4.2 and has negative charge at higher pH values than 4.35 due to its ionization (Bagal and Gogate, 2014; dos Reis et al., 2023a). Fig. 5b shows a small decrease in the S-DCF removal was observed under alkaline pH, for both biochars because both adsorbent and adsorbate have negative charges at these pH values and hence electrostatic repulsive interaction would act more effectively compared to under acid pHs. When the value of the S-DCF solution pH is higher than the pH_{pzc}, the S-DCF removal suffers a decrease, possibly because the electrostatic repulsion that happens between both the negatively charged biochars' surfaces and the S-DCF negatively charged molecules (Xie et al., 2023a, b).

This result strongly indicates that the electrostatic mechanism should not play a great influence in the adsorption process because it is highly dependent on the pH, which was not the case here. However, a small influence of the pH is observed suggesting that electrostatic attraction was also involved in the process but in less extent (dos Reis et al., 2023a). Considering these results, further adsorption tests (kinetics and isotherms) were done using S-DCF solutions at pH 6.0 (the same pH as deionized water).

3.3. Kinetic, equilibrium, thermodynamic and mechanism of adsorption

3.3.1. Kinetic studies

In the adsorption process, the kinetics play a huge importance in properly understanding the adsorption mechanism between specific adsorbate-adsorbent systems. Fig. 6 displays the kinetic curves of adsorption for S-DCF on biochar adsorbents. Both curves show similar trends regardless of S-doping, however, the S-doped biochar presented higher uptake values at the referenced times, which would be a reflex of the presence of more S-functionalities, which could serve as adsorption active sites to boost its adsorptive properties.

The kinetic of adsorption was further evaluated by assessing the suitability of the kinetic models regarding R^2_{Adj} and SD (dos Reis et al., 2021a, b; Teixeira et al., 2021; Salomon et al., 2020; Gonzalez-Hourcade

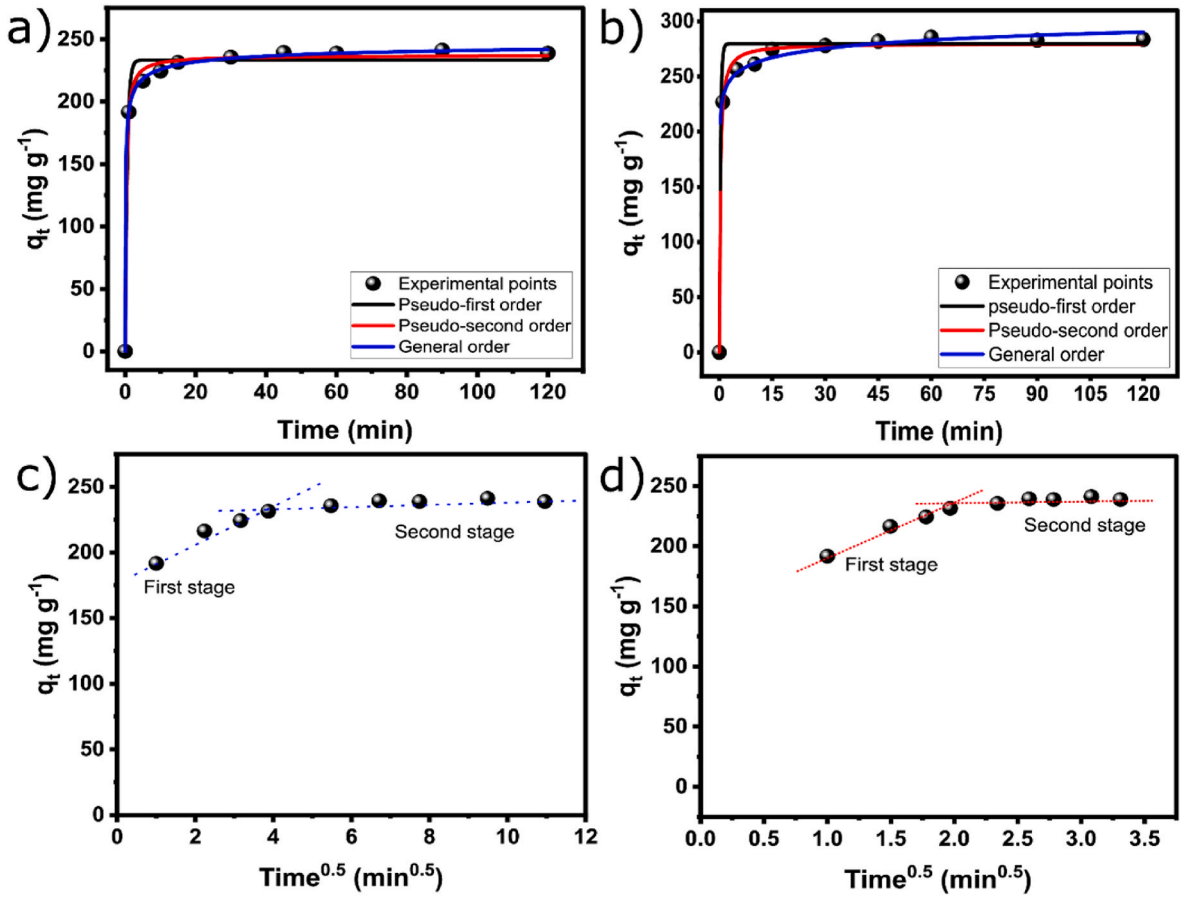

Fig. 6. Kinetic curves S-DCF adsorption on biochar adsorbents at a C_o of 500 mg L^{-1}. a) Non-doped biochar; b) S-doped biochar; c) intra-particle curve for non-doped biochar; d) intra-particle curve for S-doped biochar.

et al., 2022). The most suitable model must have a higher R^2_{Adj} and lower SD values, which indicate a smaller disparity between the q measured experimentally and theoretical q values obtained by the models. Thus, it can be concluded that General order was the model that better described the relation between S-DCF and non-doped and S-doped biochars due to its highest and lowest values for R^2_{Adj} and SD, respectively (see Table 3).

The General order's fitting points to an adsorption process order that proceeds as a chemical reaction, possibly being measured only experimentally (dos Reis et al., 2023a,b; Gonzalez-Hourcade et al., 2022). In addition, general order may present different n values (order of adsorption rate), depending on the adsorbate's concentration, which is difficult to be measured. Thus, to help to further understand the behaviour of the kinetics of S-DCF on the biochars, it is calculated and evaluated the initial sorption rate h_0 (Gonzalez-Hourcade et al., 2022; Ho, 2006). The initial sorption rate is presented in Eq. (1): $h_0 = k_n . q_e^n$. (for the details of the equation, see supplementary material).

Since General order displayed better suitability, more accurate h_0 values are obtained from it. The h_o values were 43.0 and 78.4 for non-doped and S-doped biochar, respectively (see Table 3); meaning that the kinetic process was faster in S-doped biochar compared to non-doped, which could be reflexes of the more active adsorption sites present in S-doped material.

Further evaluation of the kinetic process is shown in Fig. 6c and d (intraparticle diffusion curves). Adsorption is a multi-step process, which involves the migration/diffusion of S-DCF molecules in the solution to the biochar's surfaces/pores. Since both biochar adsorbents exhibited very porous features is likely that the inner pore diffusion played an important role in the adsorption process. The intra-particle curves exhibited two stages of adsorption (Fig. 6c and d). The first stage is related to boundary and intraparticle diffusion into the bichar pores, which seems to be faster in S-doped biochar, which can be explained by the higher number of mesopores (see Table 1). Mesopores, due to their wider size, facilitate liquid diffusion in comparison to the micropores and this in turn facilitates S-DCF penetration and adsorption. Besides, as discussed earlier, S-doped biochar has more active adsorption sites due to the abundant S-functionalities, and this also contributes to the first stage of the kinetic. In the second stage, the S-DCF was adsorbed and diffused into the interior site of the biochars until the equilibrium was attained.

3.3.2. Equilibrium of adsorption

The isotherm of adsorption are helpful approach to describe and understand how an adsorbate interacts with an adsorbent, giving useful insights about the adsorption interactions/characteristics of S-DCF on biochars. Many isotherm models are available, however Langmuir, Freundlich, and Liu were used to study the experimental measurements.

Table 3
Kinetic parameters for DCF adsorption.

	Non-doped biochar	S-doped biochar
Pseudo-first-order		
q_e (mg/g)	233	270
k_1 (1/min)	1.72	50.7
R^2_{adj}	0.987	0.957
SD (mg/g)	8.17	19.2
Pseudo-second-order		
q_e (mg/g)	237	280
k_2 (g/mg min)	0.0162	0.0138
R^2_{adj}	0.995	0.994
SD (mg/g)	4.87	6.61
General order		
q_n (mg g^{-1})	252	416
k_n (min^{-1} (g $mg^{-1})^{n-1}$)	4.5×10^{-8}	9.11×10^{-32}
n	3.74	13.3
R^2_{adj}	0.999	0.996
h_o	43.0	74.8
SD (mg g^{-1})	1.87	0.780

Their curves and parameters at different temperatures (298 K, 308 K and 318 K) are shown in Fig. 7 and Table 4. The suitability of isotherm models was explored using a similar approach to the kinetic studies (through SD and R^2_{Adj}). In this sense, Liu provided the highest R^2_{Adj} and the lowest SD values at the three employed temperatures (see Table 4), suggesting that the q fitted by the Liu isotherm model was the closest to the experimental data.

The suitability of the Liu model may indicate that the active adsorption sites on the biochar surfaces do not possess the same energy, which makes sense since biochars have different surface functionalities and have more heterogeneous characteristics. Comparing all three models, the Langmuir model was shown to be the most unsuitable because it gave the lowest and highest R^2_{adj} and SD values. On the other hand, Freundlich presented SD and R^2_{adj} values closer to Liu's values, suggesting a certain level of heterogeneity in the adsorption of S-DCF on both biochars.

3.3.3. Comparison between adsorption capacities of the S-doped biochar and other adsorbents

The results have shown excellent affinity between S-doped biochar and S-DCF molecules. However, to clearly understand the biochar effectiveness in adsorbing S-DCF it is necessary to compare its results with other adsorbents reported in the literature (dos Reis et al., 2023; Obeso et al., 2023; Rigueto et al., 2021; Zhao et al., 2016; dos Reis et al., 2016; de Souza dos Santos et al., 2020; S. Zhang et al., 2022; Hua et al., 2019; Xu et al., 2020; Álvarez et al., 2015). Therefore, aiming to assess their efficacy, the adsorption data are compared with other different adsorbents (Table 5). The q_{max} of S-doped biochar presented the highest adsorption capacity among all adsorbents shown in Table 5. To better understand how excellent the S-doped biochar adsorption performance in adsorbing S-DCF was, it is compared to the performance of Al (III)-based MOF (MOF-303) (Obeso et al., 2023) that adsorbed 334.89 mg g^{-1}, much lower than S-doped biochar (693 mg g^{-1}); furthermore, Al (III)-based MOF (MOF-303) presents a much more complex synthesis route, which implies in higher costs in the adsorption process when compared to the S-doped biochar adsorption system. The same logic is followed for the adsorption of S-DCF on Commercial gelatin/CNT's beads (Rigueto et al., 2021), which exhibited an even lower adsorption capacity 26.97 mg g^{-1}. Therefore, considering the complexity of the adsorption preparation and its respective adsorption efficiency, S-doped biochar can be considered a highly effective adsorbent for emerging pollutant removal.

3.3.4. Thermodynamic studies

The effect of the temperature was further evaluated by employing the thermodynamic studies using the thermodynamic parameters such as Gibb's free energy change (ΔG°), enthalpy change (ΔH°), and entropy change (ΔS°), these quantities help to understand the adsorption system/mechanism in relation to the magnitude and spontaneity of the adsorption system.

Calculated thermodynamic data for S-DCF uptake on biochars are presented in Table 6. ΔG° negative values indicate that the removal of S-DCF ion non-doped biochars and S-doped biochar were spontaneous (dos Reis et al., 2023; Maia et al., 2019; Lima et al., 2019; dos Reis et al., 2022a,b). ΔH° was positive indicating an endothermic nature of DCF adsorption on both biochars, explaining adsorption capacity increased with higher temperatures. The positive values of ΔH° confirmed the thermodynamic feasibility of this adsorption process. The negative ΔS° values indicate an increase in randomness at the biochars/S-DCF interface in solution and might indicate an increase in the degree of freedom of S-DCF molecules (dos Reis et al., 2023; Lima et al., 2019; dos Reis et al., 2022a,b). Similar thermodynamic behaviour was reported by Maia and co-workers (Maia et al., 2019), who studied the adsorption of S-DCF removal on commercial organoclay adsorbents.

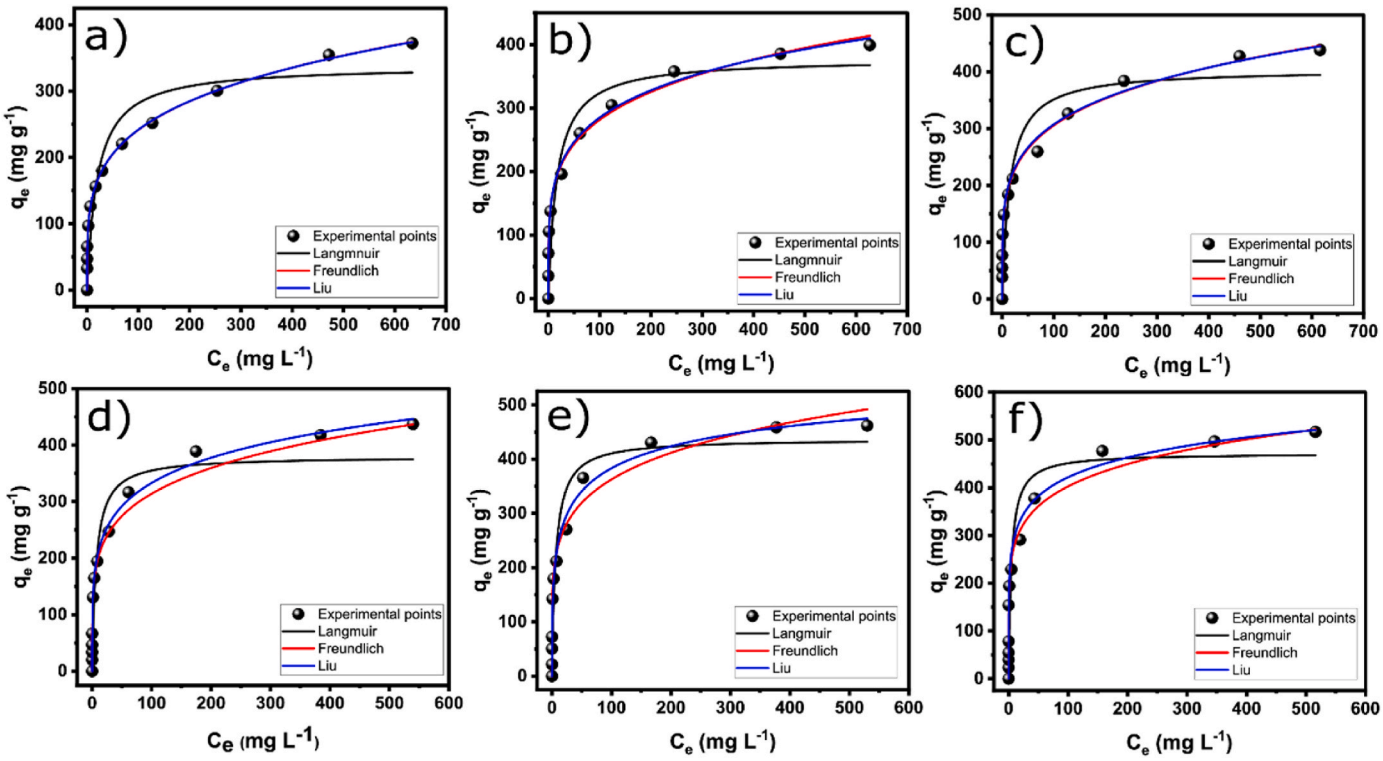

Fig. 7. Equilibrium curves of S-DCF on biochar adsorbents at different temperatures; non-doped biochar, a) 298 K; b) 308 K; c) 318 K, S-doped biochar, d) 298 K; e) 308 K; f) 318 K.

Table 4
Isotherm parameters for adsorption of S-DCF on biochar adsorbents.

Non-doped biochar	298 K	308 K	318 K
Langmuir			
q_{max} (mg/g)	338	377	404
K_L (L/min)	0.496	0.600	0.666
R^2_{adj}	0.892	0.888	0.857
SD (mg/g)	42.4	48.3	57.1
Freundlich			
K_F ((mg/g) (mg/L)$_F^{-1/n}$)	81.0	107	117
n_F	4.22	4.76	4.81
R^2_{adj}	0.996	0.988	0.973
SD (mg/g)	6.42	16.0	24.6
Liu			
q_{max} (mg/g)	493	531	564
K_g(L/mg)	0.00120	0.00833	0.0166
n_s	0.239	0.245	0.204
R^2_{adj}	0.998	0.991	0.988
SD (mg/g)	5.89	11.6	19.6
S-doped biochar			
Langmuir			
q_{max} (mg/g)	380	437	472
K_L (L/min)	0.143	0.154	0.216
R^2_{adj}	0.900	0.878	0.861
SD (mg/g)	47.8	56.2	70.5
Freundlich			
K_F ((mg/g) (mg/L)$_F^{-1/n}$)	128	156	195
n_F	5.11	5.47	6.34
R^2_{adj}	0.985	0.937	0.964
SD (mg/g)	18.5	39.11	35.3
Liu			
q_{max} (mg/g)	585	647	693
K_g (L/mg)	0.0034	0.0264	0.0467
n_s	0.263	0.384	
R^2_{adj}	0.990	0.972	0.977
SD (mg/g)	16.7	30.7	27.9

3.3.5. Regeneration and reusability tests

The regeneration and reusability of the adsorbent materials are important steps for evaluating the real adsorption applicability of the adsorbents, which can implies in the process affordability and sustainability. Both biochars (non-doped and S-doped) were employed in consecutive adsorption–desorption tests. The desorption tests were proceeded as the same procedure of the adsorption tests (50 mg of the S-DCF loaded biochar was put in contact with the eluent (0.25 M of NaOH + 20% Ethanol, 150 rpm of stirring for 2 h). After the test, S-DCF in the desorbed solution was quantified (after each adsorption step) by UV–vis spectrophotometry. Fig. 8 displays the desorption-adsorption cycles of S-DCF on Non-doped biochar and S-doped biochar adsorbents. It can be seen that the adsorption capacities of both samples exhibited a small decrease but they still kept very good sorption efficiency even after six cycles (see Fig. 9), highlighting the adsorbents' stability over successive adsorption and desorption cycles. Comparing both biochars, the S-doped biochar exhibited better cyclability performance indicating that the introduction of sulfur atoms in the carbon network enhanced the adsorption stability of the adsorbent. These results strongly suggest that the S-doping process created an adsorbent with very good recyclability performance showing that it can be used multiple times, giving to the adsorption process a more sustainable and environment-friendly status.

3.3.6. S-DCF adsorption mechanisms on sulfur-doped biochar

Based on literature adsorption data and physicochemical characterization of the carbon materials, we speculate the possible mechanism of adsorption involved in the S-DCF removal. Due to fact that both carbon materials are highly porous, with high SSA and mesopore features, the primary adsorption mechanism should be the pore filling (dos Reis et al., 2023; dos Reis et al., 2023). For instance, S-DCF has a molecule size of nearly 1.012 nm, which can easily be adsorbed and diffused into mesopores (between 2 and 50 nm). However, besides pore filling, the S-doped biochar has abundant surface functionalities that serve as active adsorption sites to bind the S-DCF molecules through electrostatic interaction, hydrogen bonding, π-π and Lewis acid-base interactions as

Table 5
Comparison between adsorption capacities of the S-doped biochar and other adsorbents.

Adsorbent	Adsorbent dosage (g L^{-1})	pH	Temperature (°C)	Q_{max} (mg g^{-1})	Ref.
Selenium doped biochar	1.0	6.5	25	355	dos Reis et al., 2023
Al(III)-based MOF (MOF-303)	1.0	7.0	25	334.89	Obeso et al. (2023)
Al(III)-based MOF (DUT-5)	1.0	7.0	25	103.36	Obeso et al. (2023)
Commercial gelatin/CNT's beads	2.0	8.15	25	26.97	Rigueto et al. (2021)
RCTLW gelatin/CNT's beads	2.0	8.15	25	20.57	Rigueto et al. (2021)
Multi-walled carbon nanotubes				157	Zhao et al. (2016)
sludge activated carbon	1.5	6.0	25	92.7	dos Reis et al. (2016)
MgAl/layered double hydroxide supported on	0.05	5.0	60	168	de Souza dos Santos et al. (2020)
$MnFe_2O_4$-magnetic biochar	0.15	4.0	25	344.26	Zhang et al. (2022)
Cellulose nanocrystals/chitosan composite	1.0	4.5	25	444	Hua et al. (2019)
Plant-based activated biochar	0.12	6.0	20	23.25	Xu et al. (2020)
Carbon xerogels	–	6.0	25	80.0	Álvarez et al. (2015)
Non-doped biochar	1.5	6.0	45	564	**This work**
S-doped biochar	1.5	6.0	45	693	**This work**

Table 6
Thermodynamic parameters of S-DCF on biochar adsorbents.

T (K)	ΔG^0 (kJ mol^{-1})	ΔH^0 (kJ mol^{-1})	ΔS^0 (kJ mol^{-1} K^{-1})
Non-doped biochar			
298	−30.54	43.2	−41.2
308	−30.88		
318	−30.71		
328	−29.15		
Sulfur-doped biochar			
298	−30.80	41.0	−33.5
308	−30.88		
318	−30.53		
328	−29.77		

illustrated in Fig. 9. Since the pH of the S-DCF solution did not have huge effect on its removal, we can state that the electrostatic interactions was not the main one of the main mechanism involved in the process, although it played some influence. Another possible mechanism could involve the hydrogen bonding between H of the S-DCF molecules and O, H, and S atoms of the biochar (Xie et al., 2023a,b) (see Fig. 9).

The S-DCF has a carboxyl group (-COOH) that can create a strong electron-withdrawing effect on the aromatic ring from the biochar, which allows the aromatic ring to bind to the electron donor biochar surfaces that establish π-π interactions (de Azevedo et al., 2023). Therefore, it is stated that the main mechanisms involved in the S-DCF adsorption are listed as the pore-filling effect, electrostatic attraction, π-π EDA interaction, and H-bonding (Fig. 8).

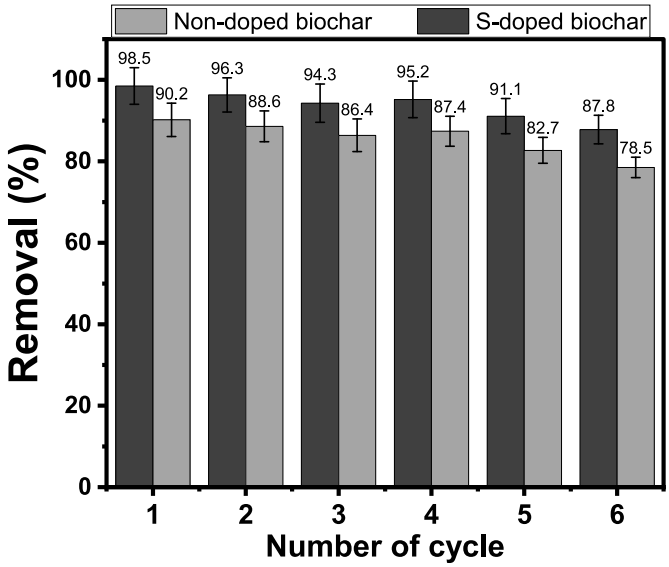

Fig. 8. Regeneration and reusability tests of Non-doped and S-doped biochars over six cycles of S-DCF adsorption–desorption.

4. Conclusion

In this work, the effect of sulfur doping on biochar physicochemical properties as well as on its adsorption performance in removing S-DCF were fully investigated. The elemental composition showed that the S-doped has 7.33% of sulfur in its structure while non-doped biochar presented only 0.153%. The higher S content had a great impact on S-doped biochar structural and surface properties. The S-doped biochar showed to have a more hydrophilic surface and lower pH_{pzc} value compared to non-doped biochar. Moreover, the higher presence of S was responsible for introducing more structural defects as showed by Raman analysis. The modification of the S-doped biochar properties positively affected its adsorptive properties. The kinetic results of S-DCF was much faster in S-doped biochar and it presented the highest adsorption capacity. The adsorption data showed that General and Liu models offered the best fitness for the kinetic and equilibrium studies, respectively. The S-doped biochar exhibited a maximum adsorption capacity of 693 mg g^{-1}at 318 K while non-doped presented 564 mg g^{-1}at 318 K, evidencing the better affinity of S-doped biochar for S-DCF molecule compared to non-doped biochar. The thermodynamic parameters (ΔH^0, ΔS^0, ΔG^0) suggested that the S-DCF removal on both adsorbents were spontaneous, favourable, and endothermic.

CRediT authorship contribution statement

Glaydson S. dos Reis: Writing – original draft, Methodology, Investigation, Formal analysis, Data curation, Conceptualization. **Alejandro Grimm:** Writing – review & editing, Formal analysis. **Denise Alves Fungaro:** Writing – review & editing. **Tao Hu:** Writing – review & editing, Formal analysis. **Irineu A.S. de Brum:** Writing – review & editing, Formal analysis. **Eder C. Lima:** Writing – review & editing. **Mu Naushad:** Writing – review & editing. **Guilherme L. Dotto:** Writing – review & editing. **Ulla Lassi:** Writing – review & editing.

Declaration of competing interest

The authors declare the following financial interests/personal

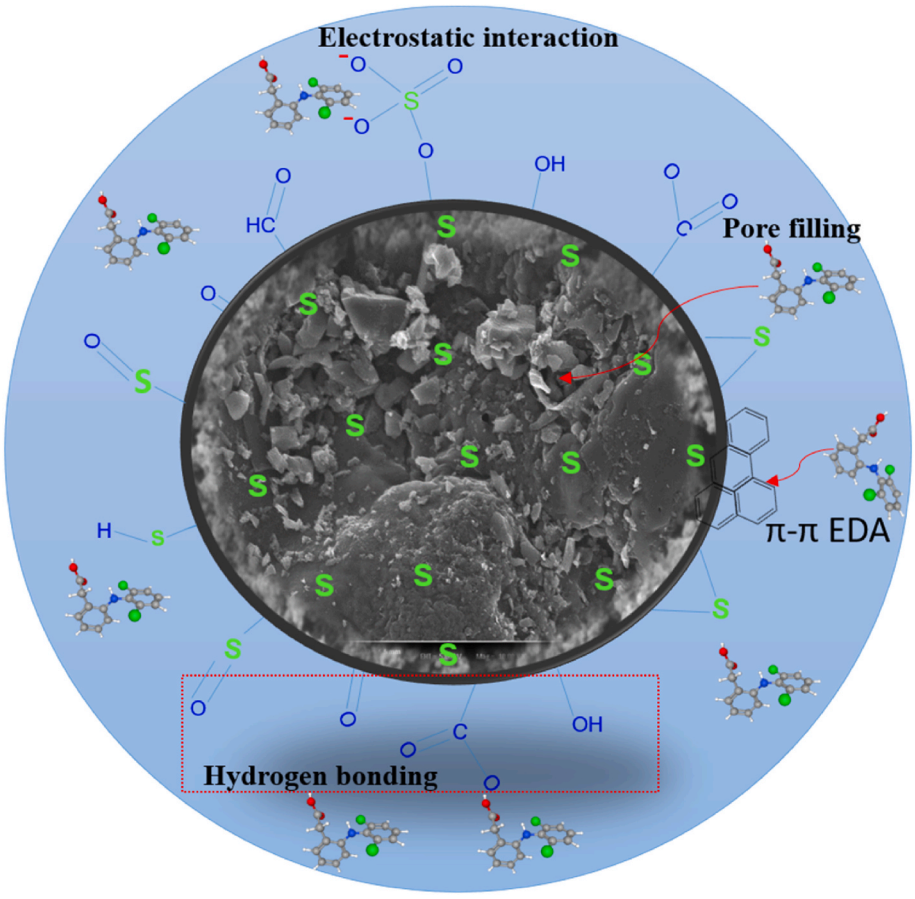

Fig. 9. Schematic of the S-DCF adsorption mechanism on S-doped biochar.

relationships which may be considered as potential competing interests: Glaydson Simoes dos Reis reports financial support was provided by Swedish University of Agricultural Sciences. If there are other authors, they declare that they have no known competing financial interests or personal relationships that could have appeared to influence the work reported in this paper.

Data availability

Data will be made available on request.

Acknowledgments

The authors wish to thank Bio4Energy, a strategic research environment appointed by the Swedish government, as well as the Swedish University of Agricultural Sciences for supporting this work. Financial support from Interreg Aurora (grant No. 20361711), the Swedish Research Council Formas (grant No. 2021–00877), and Kempes Foundation (grant No. JCSMK23-0145) is gratefully acknowledged. The Umeå Core Facility for Electron Microscopy (UCEM-NMI node) and the Vibrational Spectroscopy Core Facility (ViSp) at the Chemical Biological Centre (KBC), Umeå University, are acknowledged. The authors wish to thank A. Gorzsas for support with Raman measurements and A. Shchukarev for support with the XPS measurements. The authors thank CNPq, FINEP, and CAPES from Brazil for partially supporting this research. In addition, the authors are also grateful to the Researchers Supporting Project number (RSP 2024R8), King Saud University, Riyadh, Saudi Arabia, for the financial support.

Appendix A. Supplementary data

Supplementary data to this article can be found online at https://doi.org/10.1016/j.envres.2024.118595.

References

Ahsani, M., Hazrati, H., Javadi, M., Ulbricht, M., Yegani, R., 2020. Preparation of antibiofouling nanocomposite PVDF/Ag-SiO2 membrane and long-term performance evaluation in the MBR system fed by real pharmaceutical wastewater. Sep. Purif. Technol. 249, 116938.

Alimohammadi, P., Nejad, M.S., Miroliaei, M.R., Sheibani, H., 2022. Oriented growth of copper & nickel-impregnated δ -MnO2 nanofilaments anchored onto sulfur-doped biochar template as hybrid adsorbents for removing phenolic compounds by adsorption-oxidation process. Chem. Eng. Process. - Process. Intensif. 176, 108971.

Álvarez, S., Ribeiro, R.S., Gomes, H.T., Sotelo, J.L., García, J., 2015. Synthesis of carbon xerogels and their application in adsorption studies of caffeine and diclofenac as emerging contaminants. Chem. Eng. Res. Des. 95, 229–238.

Bagal, M.V., Gogate, P.R., 2014. Degradation of diclofenac sodium using combined processes based on hydrodynamic cavitation and heterogeneous photocatalysis. Ultrason. Sonochem. 21, 1035–1043. https://doi.org/10.1016/j.ultsonch.2013.10.020.

Correa, C.R., Otto, T., Kruse, A., 2017. Influence of the biomass components on the pore formation of activated carbon. Biomass Bioenergy 97, 53–64.

de Azevedo, C.F., Machado, F.M., de Souza, N.F., Silveira, L.L., Lima, E.C., Andreazza, R., Bergamnn, C.P., 2023. Comprehensive adsorption and spectroscopic studies on the interaction of carbon nanotubes with diclofenac anti-inflammatory. Chem. Eng. J. 454, 140102.

de Souza dos Santos, G.E., Ide, A.H., Duarte, J.L.S., McKay, G., Silva, A.O.S., Meili, L., 2020. Adsorption of anti-inflammatory drug diclofenac by MgAl/layered double hydroxide supported on Syagrus coronata biochar. Powder Technol. 364, 229–240.

Della-Flora, A., Wilde, M.L., Thue, P.S., Lima, D.R., Lima, E.C., Sirtori, C., 2020. Combination of solar photo-Fenton and adsorption process for removal of the anticancer drug Flutamide and its transformation products from hospital wastewater. J. Hazard Mater. 396, 122699.

Dionisi, D., Etteh, C.C., 2019. Effect of process conditions on the aerobic biodegradation of phenol and paracetamol by open mixed microbial cultures. J. Environ. Chem. Eng. 7, 103282 https://doi.org/10.1016/j.jece.2019.103282.

dos Reis, G.S., Mahbub, M.K.B., Wilhelm, M., Lima, E.C., Sampaio, C.H., Saucier, C., Dias, S.L.P., 2016. Activated carbon from sewage sludge for removal of sodium diclofenac and nimesulide from aqueous solutions. Kor. J. Chem. Eng. 33, 3149–3161.

dos Reis, G.S., Lima, E.C., Sampaio, C.H., Rodembusch, F.S., Petter, C.O., Cazacliu, B.G., Dotto, G.L., Hidalgo, G.E.N., 2018. Novel kaolin/polysiloxane based organicinorganic hybrid materials: sol-gel synthesis, characterisation, and photocatalytic properties. J. Solid State Chem. 260, 106–116.

dos Reis, G.S., Larsson, S.H., Thyrel, M., Pham, T.N., Lima, E.C., de Oliveira, H.P., Dotto, G.L., 2021a. Preparation and application of efficient biobased carbon adsorbents prepared from spruce bark residues for efficient removal of reactive dyes and colors from synthetic effluents. Coatings 11, 772.

dos Reis, G.S., Lima, R.A.P., Larsson, S.H., Subramaniyam, C.M., Dinh, V.M., Thyrel, M., de Oliveira, H.P., 2021b. Flexible supercapacitors of biomass-based activated carbon-polypyrrole on eggshell membranes. J. Environ. Chem. Eng. 9, 106155.

dos Reis, G.S., Guy, M., Mathieu, M., Jebrane, M., Lima, E.C., Thyrel, M., Dotto, G.L., Larsson, S.H., 2022a. A comparative study of chemical treatment by MgCl2, ZnSO4, ZnCl2, and KOH on physicochemical properties and acetaminophen adsorption performance of biobased porous materials from tree bark residues. Colloids Surf. A Physicochem. Eng. Asp. 642, 1–13. https://doi.org/10.1016/j.colsurfa.2022.128626.

dos Reis, G.S., Pinto, D., Lima, E.C., Knani, S., Grimm, A., Silva, L.F.O., Cadaval Jr., T.R. S., Dotto, G.L., 2022b. Lanthanum uptake from water using chitosan with different configurations. React. Funct. Polym. 180, 105395.

dos Reis, G.S., Thivet, J., Laisné, E., Srivastava, V., Grimm, A., Lima, E.C., Bergna, D., Hu, T., Naushad, M., Lassi, U., 2023a. Synthesis of novel mesoporous selenium-doped biochar with high-performance sodium diclofenac and reactive orange 16 dye removals. Chem. Eng. Sci. 281, 119129 https://doi.org/10.1016/j.ces.2023.119129.

dos Reis, G.S., Bergna, D., Grimm, A., Lima, E.C., Hu, T., Naushad, Mu, Lassi, U., 2023b. Preparation of highly porous nitrogen-doped biochar derived from birch tree wastes with superior dye removal performance. Colloids Surf. A Physicochem. Eng. Asp. 669, 131493 https://doi.org/10.1016/j.colsurfa.2023.131493.

dos Reis, G.S., Larsson, S.H., Thyrel, M., Mathieu, M., Tung, P.N., 2023c. Application of design of experiments (DoE) for optimised production of micro-and mesoporous Norway spruce bark activated carbons. Biomass. Conv. Bioref. 13, 10113–10131. https://doi.org/10.1007/s13399-021-01917-9.

Du, W., Zhang, Q., Shang, Y., Wang, W., Li, Q., Yue, Q., Gao, B., Xu, X., 2020. Sulfate saturated biosorbent-derived Co-S@NC nanoarchitecture as an efficient catalyst for peroxymonosulfate activation. Appl. Catal., B 262, 118302.

Gao, Y., Wang, Q., Ji, G., Li, A., Niu, J., 2021. Doping strategy, properties and application of heteroatom-doped ordered mesoporous carbon. RSC Adv. 11, 5361–5383.

Gonzalez-Hourcade, M., dos Reis, G.S., Grimm, A., Dinh, V.M., Lima, E.C., Larsson, S.H., Gentili, F.G., 2022. Microalgae biomass as a sustainable precursor to produce nitrogen-doped biochar for efficient removal of emerging pollutants from aqueous media. J. Clean. Prod. 348, 131280.

Ho, Y.S., 2006. Review of second-order models for adsorption systems. J. Hazard Mater. 136, 681–689.

Hua, D., Huanga, H., Jianga, R., Wang, N., Xu, H., Wang, Y.-G., Ouyang, X.-K., 2019. Adsorption of diclofenac sodium on bilayer amino-functionalized cellulose nanocrystals/chitosan composite. J. Hazard Mater. 369, 483–493. https://doi.org/10.1016/j.jhazmat.2019.02.057.

Huang, M., Wang, X., Liu, C., Fang, G., Gao, J., Wang, Y., Zhou, D., 2021. Facile ball milling preparation of sulfur-doped carbon as peroxymonosulfate activator for efficient removal of organic pollutants. J. Environ. Chem. Eng. 9, 106536.

Hynynen, J., Niemistö, P., Viherä-Aarnio, A., Brunner, A., Hein, S., Velling, P., 2010. Silviculture of birch (Betula pendula Roth and Betula pubescens Ehrh.) in northern Europe. Forestry 83, 103–119.

Jayaswal, K., Sahu, V., Gurjar, B.R., 2018. Water pollution, human health and remediation. In: Water Remediation. Energy, Environment, and Sustainability, pp. 11–27. https://doi.org/10.1007/978-981-10-7551-3_2.

Kinemuchi, M., Ochiai, B., 2018. Synthesis of hydrophilic sulfur-containing adsorbents for Noble metals having thiocarbonyl group based on a methacrylate bearing dithiocarbonate moieties. Adv. Mater. Sci. Eng., 3729580 https://doi.org/10.1155/2018/3729580.

Kovacic, M., Papac, J., Kusic, H., Karamanis, P., Loncaric Bozic, A., 2020. Degradation of polar and non-polar pharmaceutical pollutants in water by solar assisted photocatalysis using hydrothermal TiO2-SnS2. Chem. Eng. J. 382, 122826 https://doi.org/10.1016/j.cej.2019.122826.

Kümmerer, K., 2001. Drugs in the environment: emission of drugs, diagnostic aids and disinfectants into wastewater by hospitals in relation to other sources - a review. Chemosphere 45, 957–969. https://doi.org/10.1016/S0045-6535(01)00144-8.

Lai, C., Gao, X.P., Zhang, B., Yan, T.Y., Zhou, Z., 2009. Synthesis and electrochemical performance of sulfur/highly porous carbon composites. J. Phys. Chem. C 113, 4712–4716.

Li, Y., Xing, B., Wang, X., 2019. Nitrogen-doped hierarchical porous biochar derived from corn stalks for phenol-enhanced adsorption. Energy Fuels 33, 12459–12468.

Lima, E.C., Hosseini-bandegharaei, A., Moreno-pirajan, J.C., Anastopoulos, I., 2019. A critical review of the estimation of the thermodynamic parameters on adsorption equilibria. Wrong use of equilibrium constant in the Van ' t Hoof equation for calculation of thermodynamic parameters of adsorption. J. Mol. Liq. 273, 425–434.

Lima, D.R., Lima, E.C., Thue, P.S., Dias, S.L.P., Machado, F.M., Seliem, M.K., Sher, F., dos Reis, G.S., Saeb, M.R., Rinklebe, J., 2021. Comparison of acidic leaching using a conventional and ultrasound-assisted method for preparation of magneticactivated biochar. J. Environ. Chem. Eng. 9, 105865 https://doi.org/10.1016/j.jece.2021.105865.

Lima, E.C., Naushad, M., Reis, G.S.D., Dotto, G.L., Pavan, F.A., Guleria, A., Seliem, M.K., Sher, F., 2022. Production of carbon-based adsorbents from lignocellulosic biomass. In: Anastopoulos, I., Lima, E.C., Meili, L., Giannakoudakis, D.A. (Eds.), Biomass-Derived Materials for Environmental Applications. Elsevier, pp. 169–192.

Maia, G.S., de Andrade, J.R., da Silva, M.G.C., Vieira, M.G.A., 2019. Adsorption of diclofenac sodium onto commercial organoclay: kinetic, equilibrium and thermodynamic study. Powder Technol. 345, 140–150.

Obeso, J.L., Viltres, H., Flores, C.V., Lopez-Olvera, A., Rajabzadeh, A.R., Srinivasan, S., Ibarra, I.A., Leyva, C., 2023. Al(III)-based MOFs adsorbent for pollution remediation: insights into selective adsorption of sodium diclofenac. J. Environ. Chem. Eng. 11, 109872.

Ojha, C.S.P., Surampalli, R.Y., Bárdossy, A., Zhang, T.C., Kao, C.-M., 2017. Sustainable water resource management: an introduction. In: Sustainable Water Resources Management, pp. 1–13.

Owa, F.D., 2013. Water pollution: sources, effects, control and management. Mediterr. J. Soc. Sci. 4, 65–68. https://doi.org/10.5901/mjss.2013.v4n8p65.

Pawlyta, M., Rouzaud, J., Duber, S., 2015. Raman microspectroscopy characterisation of carbon blacks: spectral analysis and structural information. Carbon 84, 479–490.

Piergrossi, V., Fasolato, C., Capitani, F., Monteleone, G., Postorino, G., Gislon, P., 2019. Application of Raman spectroscopy in chemical investigation of impregnated activated carbon spent in hydrogen sulfide removal process. Int. J. Environ. Sci. Technol. 16, 227–1238.

Rigueto, C.V.T., Rosseto, M., Nazari, M.T., Ostwald, B.E.P., Alessandretti, I., Manera, C., Piccin, J.S., Dettmer, A., 2021. Adsorption of diclofenac sodium by composite beads prepared from tannery wastes-derived gelatin and carbon nanotubes. J. Environ. Chem. Eng. 9, 105030.

Salomon, Y.L.O., Georgin, J., dos Reis, G.S., Lima, E.C., Oliveira, M.L.S., Franco, D.S.P., Netto, M.S., Allasia, D., Dotto, G.L., 2020. Utilization of Pacara Earpod tree (Enterolobium contortisilquum) and Ironwood (Caesalpinia leiostachya) seeds as low-cost biosorbents for removal of basic fuchsine. Environ. Sci. Pollut. Res. 27, 33307–33320.

Schweitzer, L., Noblet, J., 2018. Water contamination and pollution. Green Chem. 261–290. https://doi.org/10.1016/B978-0-12-809270-5.00011-X. Inclusive Approach.

Teixeira, R.A., Lima, E.C., Benetti, A.D., Thue, P.S., Cunha, M.R., Cimirro, N.F.G.M., Sher, F., Dehghani, M.H., dos Reis, G.S., Dotto, G.L., 2021. Preparation of hybrids of wood sawdust with 3-aminopropyl-triethoxysilane. Application as an adsorbent to remove Reactive Blue 4 dye from wastewater effluents. J. Taiwan Inst. Chem. Eng. 125, 141–152.

Xie, J., Liu, M., He, M., Liu, Y., Li, J., Yu, F., Lv, Y., Lin, C., Ye, X., 2023a. Ultra-efficient adsorption of diclofenac sodium on fish-scale biochar functionalized with H3PO4 via synergistic mechanisms. Environ. Pollut. 322, 121226 https://doi.org/10.1016/j.envpol.2023.121226.

Xie, J., Zhang, L., Luo, X., Huang, L., Gong, X., Tian, J., 2023b. Sulfur anchored on N-doped porous carbon as metal-free peroxymonosulfate activator for tetracycline hydrochloride degradation: nonradical pathway mechanism, performance and biotoxicity. Chem. Eng. J. 457, 141149.

Xu, D., Li, Z., Wang, P., Bai, W., Wang, H., 2020. Aquatic plant-derived biochars produced in different pyrolytic conditions: spectroscopic studies and adsorption behavior of diclofenac sodium in water media. Sustain. Chem. Pharm. 17, 100275.

Yu, J., Tang, T., Cheng, F., Huang, D., Martin, J.L., Brewer, C.E., Grimm, R.L., Zhou, M., Luo, H., 2021. Exploring spent biomass-derived adsorbents as anodes for lithium ion batteries. Mater. Today Energy 19, 100580. https://doi.org/10.1016/j.mtener.2020.100580.

Zahrim, A.Y., Azreen, I., Jie, S.S., Yoiying, C., Felijia, J., Hasmilah, H., Gloriana, C., Khairunis, I., 2019. Nanoparticles enhanced coagulation of biologically digested leachate. In: Nanotechnology in Water and Wastewater Treatment (Issue 2017). Elsevier Inc., pp. 205–241

Zhang, B., Mei, M., Li, K., Liu, J., Wang, T., Chen, S., Li, J., 2022. One-pot synthesis of MnFe2O4 functionalized magnetic biochar by the sol-gel pyrolysis method for diclofenac sodium removal. J. Clean. Prod. 381, 135210 https://doi.org/10.1016/j.jclepro.2022.135210.

Zhang, S., Huo, X., Xu, S., Zhang, Y., Zhang, B., Wang, M., Wang, Q., Zhang, J., 2022. Original sulfur-doped carbon materials synthesized by coffee grounds for activating persulfate to BPA degradation: the key role of electron transfer. Process Saf. Environ. 168, 1219–1234.

Zhao, H., Liu, X., Cao, Z., Zhan, Y., Shi, X., Yang, Y., Xu, J., 2016. Adsorption behavior and mechanism of chloramphenicols, sulfonamides, and non-antibiotic pharmaceuticals on multi-walled carbon nanotubes. J. Hazard Mater. 310, 235–245.

Zuccato, E., Castiglioni, S., Bagnati, R., Chiabrando, C., Grassi, P., Fanelli, R., 2008. Illicit drugs, a novel group of environmental contaminants. Water Res. 42, 961–968. https://doi.org/10.1016/j.watres.2007.09.010.